2 Phase Control of Molecular System Project

– Controlling of physical properties in molecular systems –

Project Leader: Reiji Kumai

In this project, an electronic correlation in molecular crystal systems is investigated to elucidate novel phenomena such as superconductivity, ferroelectricity, and charge ordering. One of our goals is to elucidate the origins of physical properties from crystal structural information. With this aim, we conducted crystal structure analyses of various molecular systems, including organic thin films, under different external conditions.

We have conducted numerous structural studies on bulk materials using organic single crystals, with ferroelectric materials being one of our main research targets. In addition to ferroelectrics, we have paid close attention to antiferroelectrics and paraelectrics from the standpoint of their application. For example, we have suggested that organic antiferroelectrics consisting of hydrogen-bonded supramolecular assemblies, such as squaric acid, are promising in terms of their application to energy storage devices. [1] In addition, we have demonstrated their applicability by achieving a large electrostriction in organic antiferroelectrics. [2] In this report, we introduce a new possibility of applying a paraelectric as a “metaelectric,” which demonstrates a polar structure under an electric field. [3]

2-1 Metaelectric multiphase transitions in a highly polarizable molecular crystal

Metamagnetic transitions exhibit abrupt increases in magnetization with a magnetic field and have been observed in itinerant magnets such as $Sr_3Ru_2O_7$ as well as in antiferromagnets exhibiting a field-induced spin flop. Their electric counterpart is simply a metaelectric transition, which shows a sudden increase in polarization. Although this terminology has not been explicitly used, it apparently includes the electric-field-induced phase switching phenomena in antiferroelectrics between the antipolar phase and its modified polar phase, which are closely comparable under free energy. Such field-induced metaelectric transitions typically manifest themselves by the double hysteresis loops in electric polarization (P) versus an electric field (E) curve. Herein, we demonstrate a different chemical approach to metaelectric transitions using the so-called “metadielectric” molecule, which can adjust its own dipole moments in a stepwise manner in magnitudes under the action of external stimuli. For instance, two or more subunits with switchable dipoles can make their total polarizations adjustable depending on the relative dipole orientations. Bis-(*1H*-benzimidazol-2-yl)methane (BI2C) is a bridged bis(benzimidazole) carrying two covalently linked imidazole rings. Its crystal structure comprises orthogonally crossed arrays of polar ribbons made up of a ladder-like hydrogen-bond network of fully polarized molecules during the lowest temperature phase. A structural analysis reveals that a temperature change can switch on and off the polarizations of the hydrogen-bonded molecular ribbons as desired. We also found the occurrence of single and dual metaelectric transitions during the low- and intermediate-temperature phases, respectively. The following two distinct processes are involved in the field- and temperature-induced structural changes. One is conventional “antiferroelectric” switching with a forced alignment of antiparallel dipoles, and the other is a “metadielectric” molecular transformation turning on and off the polarization of each hydrogen-bonded molecular ribbon. We also demonstrate that the coexistence of these processes inevitably causes an intriguing phenomenon in that the metaelectric multiphase transitions are reflected by the phase change interchanging the multi-domain state of a single phase and an inhomogeneously mixed state of binary phases.

The temperature-induced phase transitions were identified using differential scanning calorimetry (DSC) thermograms on polycrystalline samples (Figure 1); each of the recrystallized (#α) and sublimed (#β) specimens exhibited two pairs of exothermic and endothermic peaks at high temperatures (T_A of ~458 and 465 K) and just below room temperature (T_B of ~282 and 285 K, respectively,). Therefore, three crystal phases below the decomposition point (~582 K) are designated as I, II, and III from the high-temperature side. The crystal structure of BI2C reported by Duan *et al.* [4] has a body-centered tetragonal lattice and space group $I4_1/a$ symmetry at room temperature (Phase II). By contrast, our reexaminations of the X-ray structural analysis revealed that the genuine crystal symmetry is reduced to the monoclinic space group $P2_1/c$ (two-rank subgroup of $I4_1/a$). Phase II (point group, $2/m$) is regarded as ferroelastic, the prototype point group of which is $4/m$. This symmetry reduction is accompanied by a small deviation in angle β from a right angle to 90.531(1)°, and the unit cell parameters *a* and *c* maintain the least difference (a/c = 1.0006) close to the experimental error level. Therefore, crystal twinning as a multidomain state of ferroelasticity was easily overlooked in conventional diffraction experiments. By contrast, all as-grown crystals examined were found to be twinned by high-resolution diffraction experiments using synchrotron X-rays. A single domain form was obtained by cutting a crystal into a smaller piece, and a full structural analysis at room and low temperatures was conducted on a single crystal.

The monoclinic structure is composed of four crystallographically independent molecules (denoted as A_1, A_2, B_1, and B_2). All BI2C molecules were bent similarly at the central methylene unit. The two benzimidazole units apart from the methylene bridge are separately involved in the intermolecular hydrogen bonds. A ladder-like rib-

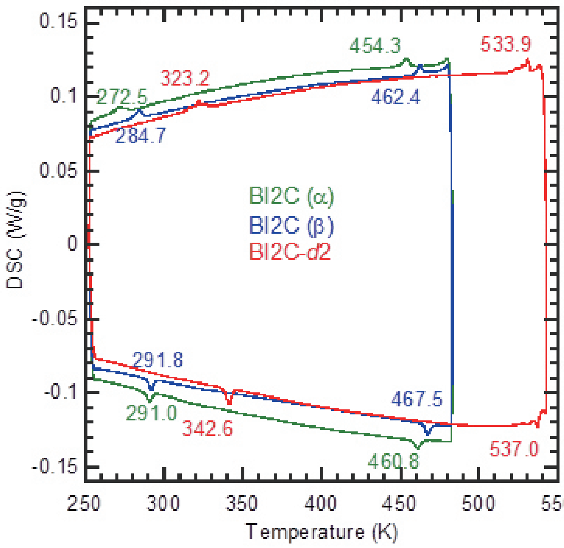

Fig. 1: Differential scanning calorimetry thermographs of BI2C: recrystallized (#α), sublimed (#β), and 91%-deuterated (BI2C-d_2) crystalline solids. Arrows indicate the directions of the temperature changes at a rate of 5 K min^{-1}.

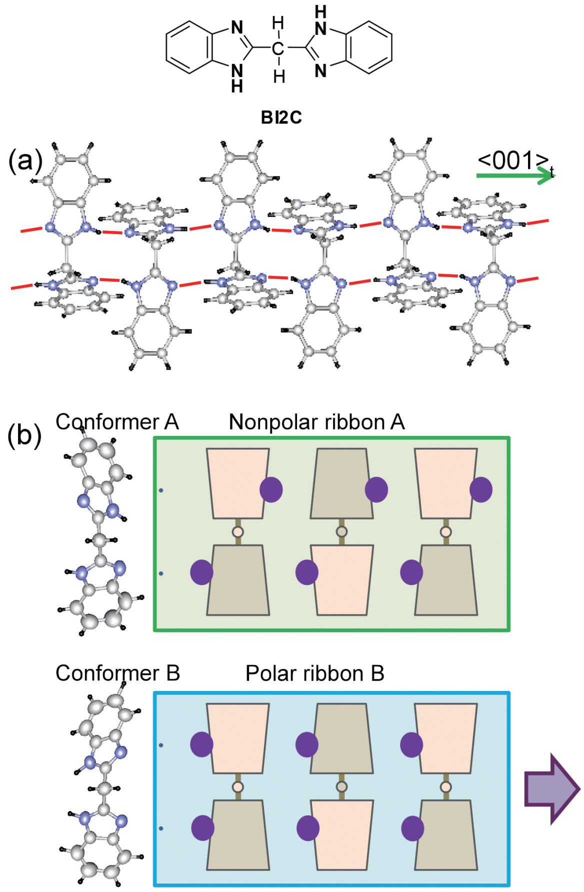

Fig. 2: Molecular structures and hydrogen-bonded arrangements in the BI2C crystals: (a) ribbon-like architectures constructed by intermolecular hydrogen bonds (solid red lines) and (b) two conformers with different NH hydrogen locations viewed along the 2-fold rotational axis of the bridging C-CH_2-C tetrahedron (left). Schematic structures of ribbons with and without local polarization (thick arrow).

bon is formed through hydrogen-bonded doublet sequences and a covalent-bonding bridge (Figure 2a). Compared with the intermolecular N…N distances in the ferroelectric or antiferroelectric benzimidazole crystals (2.80-2.97 Å), the corresponding distances in the BI2C crystal (2.77-2.86 Å) were found to be comparable or slightly shorter, and warrant field-induced prototropic switching. The ribbons are orthogonally arranged by extending parallel to either the monoclinic *a* or *c* axis (a_t or b_t axis in a tetragonal setting).

The crystal is composed of molecules of two different conformers (denoted as A and B hereafter) in a 1:1 ratio. Conformer A (i.e., molecules A_1 and A_2) adopts pseudo-C_2 symmetry, in which the orientation of the NH hydrogen atom is opposite the two benzimidazole rings when viewed along the 2-fold rotation axis of the bridging C-CH_2-C tetrahedron. Owing to the antiparallel orientation of NH hydrogen atoms, the net dipole moment of conformer A should be small along each ribbon (Figure 2b). Conformer B (molecules B_1 and B_2) adopts a similar conformation, but its pseudo-Cs-symmetry with aligned orientations of NH hydrogen atoms optimizes its dipole moment. In an actual crystal, the interconversion of one conformer to another is allowed not by a conformational isomerism but rather by proton tautomerism through hydrogen bonding, as shown below. In each molecule, two imidazolyl rings are twisted differently against the bridging C-CH_2-C, as can be seen from the difference in the corresponding CCCN torsion angles. The rotational structural flexibility around the bridge is reflected in the variations of these twisting angles with the molecules as observed.

Conformers A and B are aggregated into separate ribbons (denoted as ribbons A and B, respectively), which are orthogonal to each other. The reduction from tetragonal to monoclinic symmetry stems from the inequivalence of ribbons A and B. Ribbons A are exactly nonpolar in terms of symmetry and are parallel to the slightly longer a-axis. Ribbons B have an aligned NH orientation and strong polarization along the shorter *c*-axis. Some analogies with the magnetic system of spin $S = 1$ can be seen because the ribbons can adopt three different states in terms of the dipole moments $\boldsymbol{\mu}$: a “0” state for the nonpolar ribbons A, and a “+” or “–“ state for the dipolar ribbons B. Here, to describe the three-dimensional dipole arrangements of four ribbons in the unit cell, we adapt these symbols to the dipole moments μ_{1x} and μ_{2x} of two ribbons parallel to the a-direction and μ_{3y} and μ_{4y} of the other ribbons (see Fig. 3a). For instance, the phase II structure shown in Fig. 3b can be expressed as $\{\mu_{1x}\ \mu_{2x}\,|\mu_{3y}\ \mu_{4y}\} = \{+\ -|0\ 0\}$. The nonpolar and strongly polarized states of the ribbons should nearly degenerate under free energy, considering their coexistence in the same crystal lattice. Therefore, both the electric and thermal stimuli are expected to cause a metadielectric molecular switching of BI2C between conformers A and B. Note that the tetragonal symmetry in the raw analysis is an artifact arising from the multidomain states and represents a structure averaged over the two monoclinic crystal structures of the original and 90°-rotated configurations.

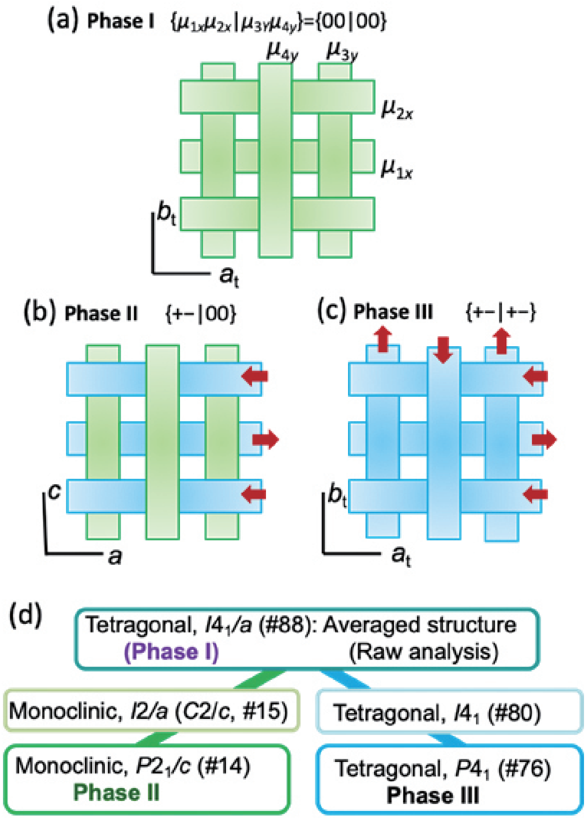

Fig. 3: Schematic three-dimensional arrangements of ribbons in (a) the raw tetragonal crystal structure (and possibly phase I), (b) true monoclinic phase II structure determined by the high-resolution, (c) phase III structure, and (d) group-subgroup interrelationship of space group symmetry between phase II and III structures.

To gain insight into the switching mechanism, we also scrutinized the temperature-induced structural transformations. Based on the observed isotope effects, the crystal structure of phase III is ready from the deuterated BI2C-d_2 crystal at room temperature. In addition, variable-temperature diffraction experiments were conducted at between 160 and 400 K on a twinning-free #α crystal using a synchrotron X-ray source. In addition, the crystal symmetry of phase I was tested at a higher temperature (of up to 468 K) using different crystal specimens.

Both the transition from phase II to phase I and from phase II to phase III are accompanied by a restoration of the tetragonal lattice symmetry (Figure 4b). The systematic absences for the phase I structure are compatible with the space group $I4_1/a$, the same as the reported (raw) room-temperature structure noted above. (A gradual sublimation of the crystal prevented data collection for a full structural analysis.) However, during phase III, systematic absences (hkl: $h + k + l = 2n + 1$) (Figure 4a) are broken, and the tetragonal lattice is not a body-centered type but a primitive type. The phase III structure at $T = 200$ K is isomorphous to that obtained from the deuterated crystal at room temperature (Figure 3c), as expected above. Although the observed systematic absences ($00l$: $l \neq 4n$) suggest the candidate non-centrosymmetric space groups of $P4_1$ (#76) and $P4_3$ (#78), the component elements C, H, and N alone do not have an anomalous X-ray dispersion effect sufficient to uniquely identify which space group represents the absolute structure. Whereas the space group symmetries of both phases II and III are the two-rank subgroup of $I4_1/a$, they are not in a group-subgroup relationship (Figure 3d), which justifies the improper ferroelectric and first-order nature of a phase transition.

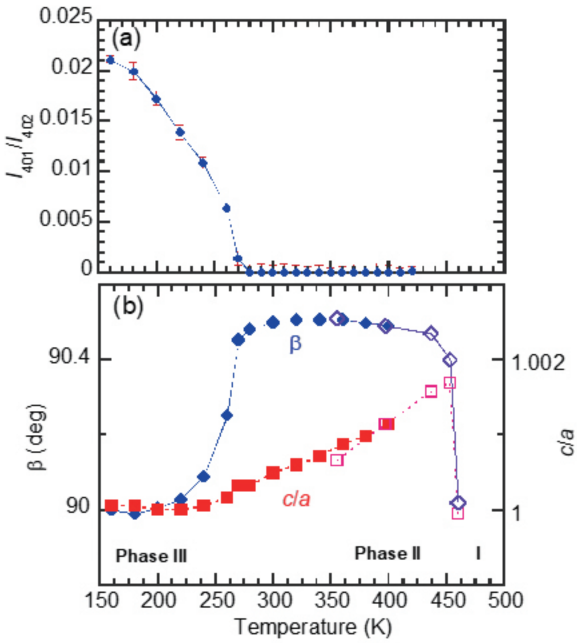

Fig. 4: Reduction of lattice symmetry of a recrystallized (#α) BI2C crystal through successive phase transitions: (a) transformation from body-centered to primitive form probed by the integrated intensity of the (401) reflection ($h + k + l =$ odd) and (b) deformation from tetragonal to monoclinic form, as demonstrated by the deviation from $\beta = 90°$ and $c/a = 1$ (dotted line). The data on the two specimens are distinguished by open and filled marks.

The crossed array of ribbons in a phase III structure is occupied solely by the strongly polarized BI2C molecules of conformer B. The 4-fold screw symmetry canceled out the strong dipole moment lying along the ribbons, constructing a $\{\mu_{1x}\ \mu_{2x}\,|\mu_{3y}\ \mu_{4y}\} = \{+\ -|+\ -\}$ structure, as schematically shown in Figure 3c. The allowed polarity is only normal to the hydrogen-bonded ribbons ($P||c_t$), and the corresponding spontaneous polarization, if present, should therefore be small. It is clear that this crystal structure has a new antiferroelectric phase distinguishable from a field-induced ferroelectric phase.

The crystal structure of deuterated BI2C-d_2 at room temperature was compared with that of BI2C to inspect how the phase II to phase III transformation is accompanied by local conformational changes of molecules in addition to the proton configurations. The representative parameters of the conformational flexibility are the CCCN torsion angles of the imidazolyl rings against the methylene bridges, as noted above and in Table S2. Among the four crystallographically independent molecules, two of them with conformer A, which are transformed into conformer B, are found to slightly increase the torsion angles ($\Delta\Phi$ of ~3° to 6°). By contrast, negligibly small changes (0.5° to 3°) are observed for the remaining two, which retain conformer B.

The temperature-dependent dielectric permittivity (Figure 5) was collected using the applied ac electric field configurations of $E||<100>_t$. Note that the crystallographic directions are represented in the pseudo-tetragonal lattice setting, as indicated by subscript "t" hereafter, considering the twinning, which mixes the tetragonal a_t and b_t axes. Using the as-grown BI2C specimens, the permittivity was also measured using a field configuration of $E \parallel \langle 101 \rangle_t$, which was tilted by 40.7° from the hydrogen-bonded sequence. The transitions between phases II and III are identified by the abrupt increase in the temperature-dependent permittivity. The permittivity jumps exhibit a pronounced thermal hysteresis, as shown in the inset of Figure 5, and are again indicative of the first-order phase transition. There are no signatures of the Curie–Weiss behavior characteristic of the proper ferroelectric or antiferroelectric phase transition. Instead, the rounded peak with a frequency dispersion of permittivity signifies the existence of dielectric relaxations at approximately 220–230 K. These anomalies are not relevant to a phase transition because neither the high-sensitivity thermal analysis nor the variable-temperature diffraction experiments detected any corresponding thermal events. Because the dielectric relaxation depends on the crystal growth conditions, its origin might be extrinsic and affected by some crystal imperfections embedded during the crystal growth and/or structural phase transition at near room temperature. The deuteration was found to significantly increase the temperature of the relaxation peak as well as the phase transition temperature (Figure 5b).

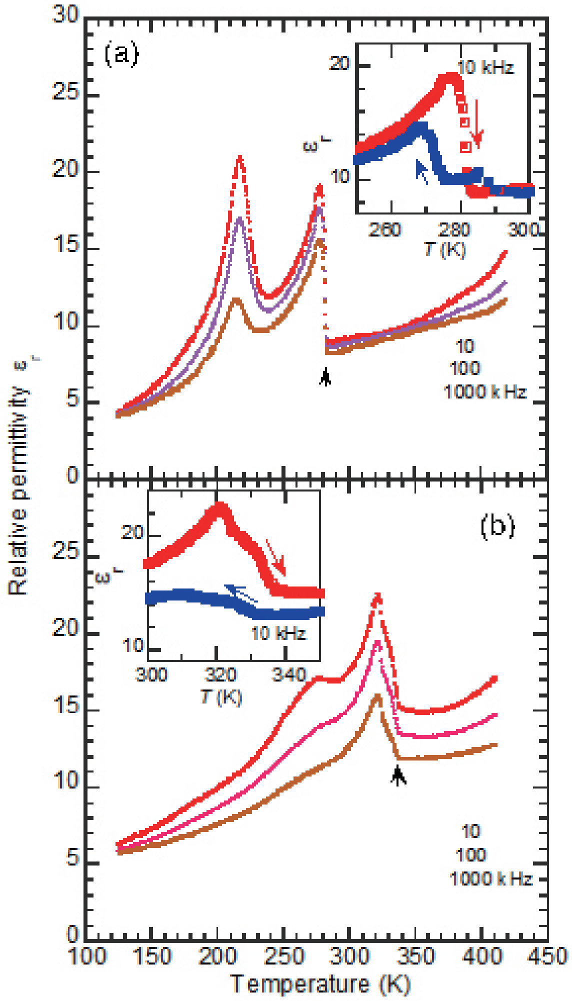

Fig. 5: Temperature-dependent relative permittivity of (a) BI2C-d_2 and (b) deuterated BI2C-d_2 crystals measured with an ac frequency of f = 10, 100, and 1,000 kHz and $E \parallel \langle 100 \rangle_t$ configuration (in the heating runs). The inset of each panel indicates the thermal hysteresis of the permittivity measured at f = 10 kHz between the cooling and heating runs.

The BI2C crystals during phase II revealed a P–E hysteresis loop characteristic of a metaelectric transition with an applied ac electric field configuration of $E \parallel \langle 101 \rangle_t$. Because most of the as-grown crystals are usually twinned by mixing the tetragonal a and b axes, each monoclinic crystal domain experiences a field configuration of either $E \parallel \langle 110 \rangle$ or $E \parallel \langle 011 \rangle$, depending on their orientation. The observed P–E hysteresis curves have no spontaneous polarization, but double hysteresis loops manifest themselves as a metaelectric transition (Figure 6a), as expected from the above

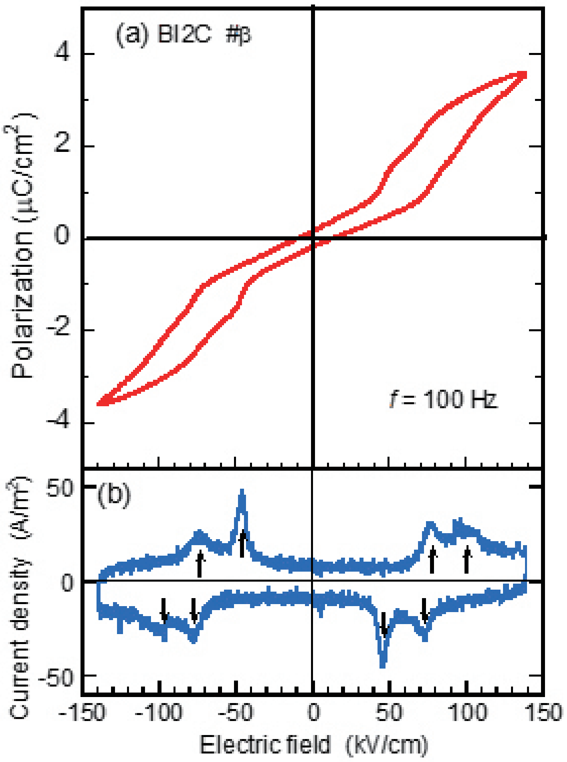

Fig. 6: Polarization switching of a sublimed BI2C (#β) crystal measured using the applied triangular waveform voltage of f = 100 Hz and $E \parallel \langle 101 \rangle_t$ configuration at room temperature (phase II): (a) P–E hysteresis loop and (b) displacement current density indicative of multiple field-induced switching obtained from the corresponding P-E hysteresis loops.

structural reassessment. The quasi-step-like polarization changes of 2.0 μC cm^{-2} emerge at a field amplitude of approximately 80 kV cm^{-1}, and the overall features do not depend on the crystal growth conditions. Attempts to detect the switchable polarizations along the $[001]_t$ direction failed, probably owing to the tiny spontaneous polarizations as theoretically predicted.

A variety of phase change phenomena have been successfully demonstrated in BI2C crystals by virtue of their metadielectric molecular properties. Here, two imidazolyl subunits accommodating each switchable dipole are covalently linked, making their total polarizations adjustable depending on the relative dipole orientations. Consequently, similar to a magnetic system with spin S = 1, the hydrogen-bonded ribbons can adopt three different states in terms of their dipole moments $\boldsymbol{\mu}$: a “0” state for the nonpolar ribbons A, and a “+” or “–“ state for the dipolar ribbons B. Two distinct switching processes are found to describe both the temperature- and field-induced structural changes. One is conventional “antiferroelectric” switching with a forced alignment of antiparallel dipoles. This mechanism is involved in the field-induced switching from both phases II and III. The other is a “metadielectric” molecular transformation turning on and off the polarization of each ribbon. The latter process is temperature-induced at T_B as well as at either of the metaelectric multiphase transitions.

The other intriguing feature of the BI2C crystals arises from ferroelastic twinning into a multi-domain state. In the applied electric field, each domain is transformed into either of the new phases, IV or V, according to the field configurations. The metaelectric multiphase transitions can be ascribed to the phase transitions II//IV and II/V occurring in the different critical fields, which interchange the multi-domain state of the single phase II and inhomogeneously mixed state of binary phases IV and V. At first glance, the BI2C crystal is similar to the SQA crystals in terms of the two-dimensional nature of the antiferroelectricity on the pseudotetragonal lattice and the symmetry reduction from a prototype to ferroelastic form. However, its microscopic switching mechanism as well as a sublattice model are quite distinct from each other.

The present study demonstrated that metadielectric molecular properties have opened the door to a rich variety of electric, thermal, and structural phases, properties, and functionalities of organic dielectrics. The design principle employed herein is quite simple, utilizing only two polar switchable subunits per molecule. For future use, there should be numerous other metadielectric molecules available because the subunits can be modified in diverse ways. It is also expected that further exotic materials should be materialized by increasing the number of subunits.

References

[1] S. Horiuchi, J. Tsutsumi, K. Kobayashi, R. Kumai, and S. Ishibashi, *J. Mater. Chem. C*, 6, 4714–4719 (2018).; S. Ishibashi, S. Horiuchi, and R. Kumai, *Phys. Rev. B*, **97**, 184102 (2018).

[2] K. Kobayashi, S. Horiuchi, S. Ishibashi, and R. Kumai, *J. Am. Chem. Soc.*, **140**, 3842–3845 (2018).

[3] S. Horiuchi, S. Ishibashi, R. Haruki, R. Kumai, S. Inada, and S. Aoyagi, *Chem. Sci.*, in press.

[4] Duan, G. -Y.; Sun, Y. -W.; Liu, J. -Z.; Wang, J. -W., *Acta Cryst. E*, **61**, o3476-o3477 (2015).